

Developing Sheet Beam Klystron Simulation Capability in AJDISK

A. Jensen, M. Fazio, J. Neilson and G. Scheitrum

Abstract—AJDISK is a 1D large signal klystron simulator developed at SLAC. A brief discussion of AJDISK’s simulation algorithm is given and [1] is fully developed to show how AJDISK was extended to enable sheet beam klystron simulations. The primary requirement for extending “disk” simulators to sheet beam simulators is a space charge equation. Therefore, the electric field due to an infinitely thin plate of charge (infinitely thin in the direction of propagation) in a rectangular drift tube is derived. The derivation is extended to a “2D” space charge equation in which the plate is split into a series of rods with varying positions in y . The derived equations are compared with numerical simulations and measurement.

Index Terms—Klystron, Sheet Beam, Simulation, Space Charge

I. INTRODUCTION

SHEET beam devices are a new class of microwave tube that have the potential to compete with multi-beam devices. Like multi-beam devices, sheet beam devices have lower current density beams and increased surface area, making them particularly suited for high power applications. Reduced cathode loading increases lifetime and lower current density beams require lower magnetic fields for focusing. Sheet beam devices require only one beam, cathode, and anode. This reduced complexity may lead to several advantages over multi-beam devices, including, fewer parts, simplified manufacturing, reduced cost, increased lifetime, and greater yield.

Drawbacks for sheet beam devices include lower cavity interaction impedance and possible mode competition, but 3D simulations can help provide insight for overcoming these challenges. The klystron group at Stanford Linear Accelerator Center (SLAC), for example, has recently designed and manufactured a working low power 95GHz sheet beam klystron [2].

3D simulations are too slow to be “good” tools for every phase in sheet beam device design. A full 3D simulation of a sheet beam klystron may take several weeks to simulate. Complimentary simulations that can reduce this design time are therefore very attractive. The disk method presented by [3] and [4] has been a common method for reducing simulation time of cylindrical beam devices, but little work has been done using this technique for sheet beam devices. This paper

extends the disk methods discussed in [3] and [4] to sheet beam klystrons and uses the results in SLAC’s AJDISK simulator to simulate sheet beam klystrons.

The primary requirement to extend a cylindrical beam simulator to a sheet beam simulator is a new space charge equation. For cylindrical beam “disk” simulators, the space charge equation is derived for a cylindrical disk of charge in a cylindrical drift tube (Fig. 1a). For sheet beam “plate” simulators, the space charge equation must be derived for a plate of charge in a rectangular drift tube (Fig. 1b). As shown in Fig. 1, disk and plate simulators can add another degree of freedom if the space charge equations for rings and rods are known. In this paper the space charge equations for plates and rods will be derived, but only for electric fields in the direction of propagation.

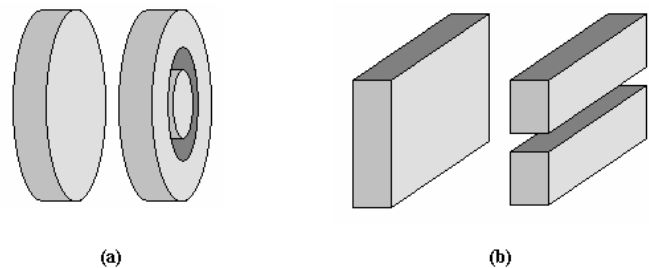


Fig. 1. (a) Disk and ring model. (b) Plate and rod model.

II. SIMULATION ALGORITHM

1D klystron simulations are discussed in depth in [3] and [4] and should be consulted for the details of the approach to be discussed.

The primary objective of a klystron simulation is self consistent RF beam interaction including space charge forces in electron bunches. The simulation splits the beam up into a series of thin rectangular plates in the direction of propagation (z in the following equations). The force on each plate is then a function of the electric field in each cavity and the space charge field from all other plates. The force equation is then solved numerically.

The equation of motion (where γ is the relativistic correction factor),

$$\bar{\mathbf{F}} = \frac{d(\gamma m \bar{\mathbf{v}})}{dt} \quad (1)$$

and the Lorentz force equation,

$$\bar{\mathbf{F}} = q(\bar{\mathbf{E}} + \bar{\mathbf{v}} \times \bar{\mathbf{B}}) \quad (2)$$

are used to describe the motion of charge (plates). If the beam is assumed to be confined by the magnetic field and only motion in z is permitted, then (1) and (2) may be combined as follows,

$$\gamma^3 m \frac{d^2 z}{dt^2} = qE_z = q(E_{cav} + E_{spch}) \quad (3)$$

Where the electric field has been separated into the electric field from the klystron cavity and the space charge field from other plates (the electric fields in (3) are in the z direction only). Once the expressions for E_{cav} and E_{spch} are known, equation (3) may be solved numerically. E_{spch} is derived in a later section of this paper and E_{cav} is given by,

$$E_{cav} = |V| f(z) \cos(\omega_0 t + \theta) \quad (4)$$

Where $|V|$ is the voltage of the cavity, $f(z)$ is the spatial shape of the electric field whose area has been normalized to one (such that $|V|$ is defined properly), ω_0 is the operating frequency of the klystron, and θ is the phase of the electric field with respect to time. A convenient analytical representation of $f(z)$ for a single gap cavity is given by [5],

$$f(z) = \frac{k}{\sqrt{\pi}} \exp[-k^2(z - z_0)^2] \quad (5)$$

Where k is the shaping coefficient of the Gaussian profile. k may be found by curve fitting, but it is more convenient to express k in terms of common klystron parameters such as the coupling coefficient (M) and the electron propagation constant (β_e),

$$k = \frac{1}{2} \frac{\beta_e}{\sqrt{-\ln(M)}} \quad (6)$$

To apply equation (4), expressions or values for $|V|$ and θ are needed. $|V|$ and θ for the input gap are given by [6], provided the input power is a known. For the remaining cavities, $|V|$ and θ are found numerically by solving (3) iteratively. After each iteration, $|V|$ and θ are calculated using Ohms law until they converge,

$$V = I_{ind,1} Z_{cav} \quad (7)$$

Where V contains both the phase and amplitude information, Z_{cav} is the cavity impedance,

$$Z_{cav} = \frac{R/Q}{\frac{1}{Q_t} + j \frac{\omega_0^2 - \omega_{cav}^2}{\omega_0 \omega_{cav}}} \quad (8)$$

and $I_{ind,1}$ is the RF current induced at the first harmonic. The first harmonic of the Fourier transform of the total induced current as a function of time is,

$$I_{ind,1} = \mathcal{F}\{I_{ind}(t)\} = \mathcal{F}\left\{\sum_i^i Q_i v_i(t) f(z_i)\right\} \quad (9)$$

The sum in (9) is over all plates, v_i is the plate velocity and Q_i is the plate charge ($I_0/(f_0 * \#Plates)$). $\#Plates$ are the number of plates in an RF cycle (typically defined by the user of the simulator).

AJDISK uses equations (3) through (9) as shown in the simplified algorithm in Fig. 2. The numerical computations are implemented in C++ and packaged as a dynamic link library so that other programs can easily use it for optimization and/or post processing. The standard GUI provided with AJDISK is written in Java.

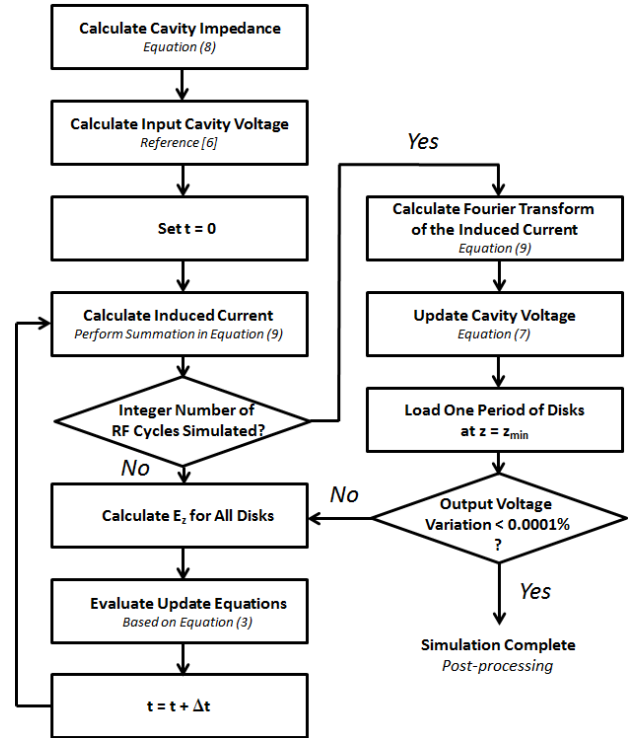


Fig. 2. Simplified AJDISK Algorithm.

AJDISK typically converges to a solution in well under a minute. The accuracy of the solution depends on the number of time steps and disks per RF cycle. Fig. 3. shows errors

typical of AJDISK simulations in general. Errors of less than 1% are shown in white. While the number of steps is important for an accurate result, it is of more importance to have enough disks to spatially represent tight bunching. Fig. 3 shows 30 to 40 disks are needed for a ~70% efficient klystron. Simulations with less than 6 time steps produced such large errors they were discarded from the chart.

		Steps (Temporal Resolution)											
		6	10	15	20	25	30	35	40	45	50	55	60
Disks (Spatial Resolution)	5	56.1	4.24	-2.09	-3.24	-2.62	-2.05	-1.37	-0.74	-1.15	0.94	1.54	1.83
	10	-71.9	-9.75	-4.72	-2.27	4.34	12.14	17.63	19.66	18.82	16.20	12.70	8.96
	15	-28.7	-4.72	2.79	8.57	-3.59	-8.96	-8.32	-7.60	-6.96	-6.42	-5.93	-5.53
	20	1.65	-2.27	4.74	-6.22	-4.60	-1.39	1.24	3.05	4.12	4.72	4.97	4.98
	25	3.51	4.34	-0.87	-1.57	2.18	2.57	1.11	-0.76	-2.30	-3.32	-3.84	-3.94
	30	-1.47	12.14	-2.10	1.25	0.27	-1.82	-2.01	-1.24	-0.43	0.20	0.67	0.98
	35	-3.18	17.63	-0.73	0.28	-1.26	-0.20	0.70	0.73	0.54	0.17	-0.20	-0.54
	40	1.01	-0.27	0.12	-0.61	0.20	0.38	-0.13	-0.61	-0.74	-0.63	-0.42	-0.20
	45	0.75	-0.09	0.37	-0.20	0.27	-0.29	-0.37	-0.04	0.19	0.29	0.29	0.18
	50	-0.10	-0.04	0.39	0.21	-0.13	-0.07	0.16	-0.14	0.02	-0.14	-0.26	-0.27
	55	-0.49	0.08	0.07	0.19	0.00	0.18	-0.03	-0.14	-0.11	-0.02	0.06	0.11
60	-0.53	0.05	0.04	0.02	0.12	0.02	-0.08	0.04	0.11	0.11	0.04	0.00	

Fig. 3. Case Study of Simulation Error in Percent with Respect to Disk and Step Count.

III. SPACE CHARGE DERIVATION

The next several sections look at the derivation of the space charge equation needed to evaluate (3), which closely follows the round beam approach in [7] and [8]. The analysis begins by deriving Green's function for a point charge in a rectangular drift tube using Laplace's equation. The Green's function is then integrated over the transverse area of the beam to generate the field of an infinitely thin sheet of charge in the direction of propagation with x and y dimensions of the beam, as shown in Fig. 4. The equation derived is then extended to 2D except that the beam sections are not allowed to have motion in y (only force in z is considered).

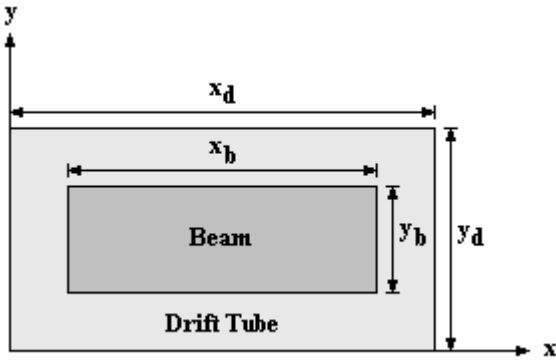


Fig. 4. Beam parameters.

IV. LAPLACE'S EQUATION

Laplace's equation states,

$$\nabla^2 V = \frac{\partial^2}{\partial x^2} V + \frac{\partial^2}{\partial y^2} V + \frac{\partial^2}{\partial z^2} V = 0 \quad (10)$$

Using the method of separation of variables,

$$V = X(x)Y(y)Z(z) \quad (11)$$

Assuming the boundary conditions $X(0)=0$, $X(x_d)=0$, and that the solution should go to zero as z goes to infinity,

$$V(x, y, z) = \sum_{m=1}^{\infty} \sum_{n=1}^{\infty} A_{mn} \sin\left(\frac{\pi m}{x_d} x\right) \sin\left(\frac{\pi n}{y_d} y\right) \cdot \exp\left[-\frac{\pi}{x_d y_d} (y_d^2 m^2 + x_d^2 n^2)^{1/2} |z|\right] \quad (12)$$

V. GREEN FUNCTION

Translating the point charge to $x=x_0$, $y=y_0$, and $z=z_0$, and since the potential should be symmetric about the point $z=z_0$,

$$V(x, y, z) = \sum_{m=1}^{\infty} \sum_{n=1}^{\infty} A_{mn}(x_0, y_0) \sin\left(\frac{\pi m}{x_d} x\right) \sin\left(\frac{\pi n}{y_d} y\right) \cdot \exp\left[-\frac{\pi}{x_d y_d} (y_d^2 m^2 + x_d^2 n^2)^{1/2} |z - z_0|\right] \quad (13)$$

From (13) we may write,

$$\frac{\partial V}{\partial z} \Big|_{z=z_0} = -\sum_{m=1}^{\infty} \sum_{n=1}^{\infty} A_{mn} \frac{\pi}{x_d y_d} (y_d^2 m^2 + x_d^2 n^2)^{1/2} \cdot \sin\left(\frac{\pi m}{x_d} x\right) \sin\left(\frac{\pi n}{y_d} y\right) \quad (14)$$

To eliminate the infinite sum we multiply both sides of (14) by orthogonal basis functions and integrate,

$$\int_0^{y_d} \int_0^{x_d} \frac{\partial V}{\partial z} \Big|_{z=z_0} \sin\left(\frac{\pi m}{x_d} x\right) \sin\left(\frac{\pi n}{y_d} y\right) dx dy = -A_{mn} \frac{\pi}{x_d y_d} (y_d^2 m^2 + x_d^2 n^2)^{1/2} \cdot \int_0^{y_d} \int_0^{x_d} \sin^2\left(\frac{\pi m}{x_d} x\right) \sin^2\left(\frac{\pi n}{y_d} y\right) dx dy \quad (15)$$

The region in the $z=z_0$ plane over which $\frac{\partial V}{\partial z} \Big|_{z=z_0} \neq 0$ is small enough that the left hand side of (15) may be written,

$$\sin\left(\frac{\pi m}{x_d}x_0\right)\sin\left(\frac{\pi n}{y_d}y_0\right)\int_0^{y_d}\int_0^{x_d}\frac{\partial V}{\partial z}\Big|_{z=z_0}dxdy \quad (16)$$

Using Gauss' theorem (16) becomes,

$$-\frac{q}{2\epsilon_0}\sin\left(\frac{\pi m}{x_d}x_0\right)\sin\left(\frac{\pi n}{y_d}y_0\right) \quad (17)$$

Now we need to evaluate the right hand side of (15) which may be rewritten,

$$-A_{mn}\frac{\pi}{x_d y_d}(y_d^2 m^2 + x_d^2 n^2)^{1/2}\int_0^{x_d}\sin^2\left(\frac{\pi m}{x_d}x\right)dx\int_0^{y_d}\sin^2\left(\frac{\pi n}{y_d}y\right)dy \quad (18)$$

Evaluating (18),

$$-A_{mn}\frac{\pi}{x_d y_d}(y_d^2 m^2 + x_d^2 n^2)^{1/2}\frac{x_d}{2}\frac{y_d}{2} = -A_{mn}\pi\frac{1}{4}(y_d^2 m^2 + x_d^2 n^2)^{1/2} \quad (19)$$

Equating (17) and (19),

$$-\frac{q}{2\epsilon_0}\sin\left(\frac{\pi m}{x_d}x_0\right)\sin\left(\frac{\pi n}{y_d}y_0\right) = -A_{mn}\pi\frac{1}{4}(y_d^2 m^2 + x_d^2 n^2)^{1/2} \quad (20)$$

Solving (20) for A_{mn} ,

$$A_{mn} = 2\frac{q}{\pi\epsilon_0}\sin\left(\frac{\pi m}{x_d}x_0\right)\sin\left(\frac{\pi n}{y_d}y_0\right)(y_d^2 m^2 + x_d^2 n^2)^{-1/2} \quad (21)$$

Combining (21) and (13),

$$V(x, y, z) = 2\frac{q}{\pi\epsilon_0}\sum_{m=1}^{\infty}\sum_{n=1}^{\infty}(y_d^2 m^2 + x_d^2 n^2)^{-1/2} \cdot \sin\left(\frac{\pi m}{x_d}x_0\right)\sin\left(\frac{\pi n}{y_d}y_0\right)\sin\left(\frac{\pi m}{x_d}x\right)\sin\left(\frac{\pi n}{y_d}y\right) \cdot \exp\left[-\frac{\pi}{x_d y_d}(y_d^2 m^2 + x_d^2 n^2)^{1/2}|z - z_0|\right] \quad (22)$$

VI. 1D SPACE CHARGE MODEL

Dropping q in (22) gives the Green's function,

$$G(x, y, z) = \frac{2}{\pi\epsilon_0}\sum_{m=1}^{\infty}\sum_{n=1}^{\infty}(y_d^2 m^2 + x_d^2 n^2)^{-1/2} \cdot \sin\left(\frac{\pi m}{x_d}x_0\right)\sin\left(\frac{\pi n}{y_d}y_0\right)\sin\left(\frac{\pi m}{x_d}x\right)\sin\left(\frac{\pi n}{y_d}y\right) \cdot \exp\left[-\frac{\pi}{x_d y_d}(y_d^2 m^2 + x_d^2 n^2)^{1/2}|z - z_0|\right] \quad (23)$$

The charge density may be written,

$$\rho = \begin{cases} \frac{Q}{A}\delta(z - z_0) & \text{for } 0 < y < y_d, 0 < x < x_d \\ 0 & \text{otherwise} \end{cases} \quad (24)$$

Where, A is the area of the beam, x_b, y_b , and Q is the charge in a plate ($I_o/(f_o * \#Plates)$).

To find the potential from a plate of charge,

$$V = \iiint_{\tau} \rho G d\tau \quad (25)$$

The Green's function already considers the delta function in z so,

$$V = \frac{Q}{A} \iint G dx_0 dy_0 \quad (26)$$

Evaluating (26) for a rectangular beam, x_b by y_b ,

$$V(x, y, z) = \frac{2}{\pi\epsilon_0} \frac{x_d y_d}{\pi^2} \frac{Q}{A} \sum_{m=1}^{\infty} \sum_{n=1}^{\infty} \frac{1}{mn} (y_d^2 m^2 + x_d^2 n^2)^{-1/2} \cdot \cos\left(\frac{\pi m}{x_d}x_0\right)\cos\left(\frac{\pi n}{y_d}y_0\right)\sin\left(\frac{\pi m}{x_d}x\right)\sin\left(\frac{\pi n}{y_d}y\right) \cdot \exp\left[-\frac{\pi}{x_d y_d}(y_d^2 m^2 + x_d^2 n^2)^{1/2}|z - z_0|\right] \Bigg|_{y_0 = \frac{y_d}{2} - \frac{y_b}{2}}^{\frac{y_d}{2} + \frac{y_b}{2}} \Bigg|_{x_0 = \frac{x_d}{2} - \frac{x_b}{2}}^{\frac{x_d}{2} + \frac{x_b}{2}} \quad (27)$$

Where, (27) is integrated over the beam. To get E_z ,

$$E_z = -\frac{\partial}{\partial z} V \quad (28)$$

From Fig. 4, the center of the beam is not at $x=0, y=0$. Using (28) on (27) and transposing the center of the beam to $(0, 0)$,

$$E_z = \frac{2}{\pi^2 \epsilon_0} \frac{Q}{A} \frac{z}{|z|} \sum_{m=1}^{\infty} \sum_{n=1}^{\infty} \frac{1}{mn} \cdot \left[\cos\left(\frac{\pi m}{2x_d}(x_d + x_b)\right) - \cos\left(\frac{\pi m}{2x_d}(x_d - x_b)\right) \right] \cdot \left[\cos\left(\frac{\pi n}{2y_d}(y_d + y_b)\right) - \cos\left(\frac{\pi n}{2y_d}(y_d - y_b)\right) \right] \cdot \sin\left(\frac{\pi n}{2y_d}(y_d + 2y)\right)\sin\left(\frac{\pi m}{2x_d}(x_d + 2x)\right) \cdot \exp\left[-\frac{\pi}{x_d y_d}(y_d^2 m^2 + x_d^2 n^2)^{1/2}|z - z_0|\right] \quad (29)$$

To calculate the average force on a plate in equation (3) it is necessary to have an expression for E_z averaged over another plate at position some δz away. To average E_z over a plate at any position z we simply integrate over the beam with respect to x and y and divide by the beam area A . Thus,

$$E_z = 2 \frac{x_d y_d}{\pi^4 \epsilon_0 A^2} \frac{Q}{|z|} \sum_{m=1}^{\infty} \sum_{n=1}^{\infty} \frac{1}{m^2 n^2} \cdot \left[\cos\left(\frac{\pi m}{2x_d}(x_d + x_b)\right) - \cos\left(\frac{\pi m}{2x_d}(x_d - x_b)\right) \right]^2 \cdot \left[\cos\left(\frac{\pi n}{2y_d}(y_d + y_b)\right) - \cos\left(\frac{\pi n}{2y_d}(y_d - y_b)\right) \right]^2 \cdot \exp\left[-\frac{\pi}{x_d y_d} (y_d^2 m^2 + x_d^2 n^2)^{1/2} |z - z_0|\right] \quad (30)$$

VII. 2D SPACE CHARGE MODEL

The 1D space charge model can be extended to a 2D space charge model by changing the limits of integration. The 2D model will be described using the parameters in Fig. 5. The beam will be split into a set of rods with bounding y positions of $y_{\min 1}$ and $y_{\max 1}$. This allows the beam to shear as a function y when $f(z)$ in equation (4) is replaced by $f(y, z)$. Since the beam is symmetric in y about $y = y_d/2$, computation time can be saved by treating each rod as a pair of rods. Where, the first rod is defined between the positions $y_{\min 1}$ and $y_{\max 1}$ and the second between $-y_{\min 1}$ and $-y_{\max 1}$. When the field for each pair of rods is averaged, the values will be averaged over $y_{\min 2}$ to $y_{\max 2}$ and $-y_{\min 2}$ to $-y_{\max 2}$.

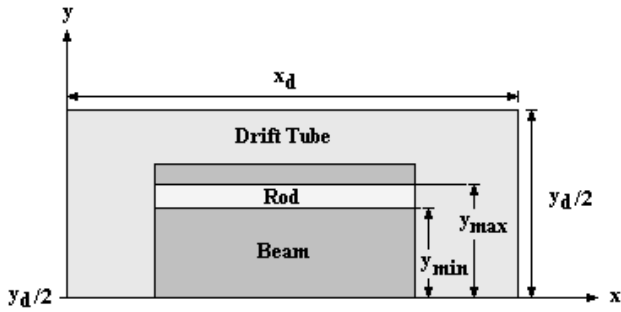


Fig. 5. 2D beam parameters.

We can start with (27) and change the limits of integration in y to find the 2D equation.

$$E_z = \frac{2}{\pi^2 \epsilon_0 A} \frac{Q}{|z|} \sum_{m=1}^{\infty} \sum_{n=1}^{\infty} \frac{1}{mn} \cdot \left[\cos\left(\frac{\pi m}{2x_d}(x_d + x_b)\right) - \cos\left(\frac{\pi m}{2x_d}(x_d - x_b)\right) \right] \cdot \left[\cos\left(\frac{\pi n}{2y_d}(y_d + 2y_{\max 1})\right) - \cos\left(\frac{\pi n}{2y_d}(y_d + 2y_{\min 1})\right) \right] + \left[\cos\left(\frac{\pi n}{2y_d}(y_d - 2y_{\min 1})\right) - \cos\left(\frac{\pi n}{2y_d}(y_d - 2y_{\max 1})\right) \right] \cdot \sin\left(\frac{\pi n}{y_d}(y_d + 2y)\right) \sin\left(\frac{\pi m}{2x_d}(x_d + 2x)\right) \cdot \exp\left[-\frac{\pi}{x_d y_d} (y_d^2 m^2 + x_d^2 n^2)^{1/2} |z - z_0|\right] \quad (31)$$

Averaging over another set of rods,

$$E_z = 16 \frac{x_d y_d}{\pi^4 \epsilon_0 A x_b (y_{\max 2} - y_{\min 2})} \frac{Q}{|z|} \sum_{m=1}^{\infty} \sum_{n=1}^{\infty} \frac{1}{m^2 n^2} \cdot \sin\left(\frac{\pi m}{2x_d} x_b\right)^2 \sin\left(\frac{\pi n}{2} y\right)^2 \cdot \left[\sin\left(\frac{\pi n}{y_d} y_{\min 1}\right) - \sin\left(\frac{\pi n}{y_d} y_{\max 1}\right) \right] \cdot \left[\sin\left(\frac{\pi n}{y_d} y_{\min 2}\right) - \sin\left(\frac{\pi n}{y_d} y_{\max 2}\right) \right] \cdot \exp\left[-\frac{\pi}{x_d y_d} (y_d^2 m^2 + x_d^2 n^2)^{1/2} |z - z_0|\right] \quad (32)$$

VIII. ANALYSIS VS SIMULATION

To check the accuracy of the analytic space charge equations, finite element Superfish simulations were done for comparison. Fig. 6 shows good agreement between the simulated fields and the theoretical fields.

For the simulated result of the average electric field in Fig. 6a., points at five positions in y were taken. In Fig. 6b., the upper half of the beam was split into three rods and only the top rod was kept. The field was then sampled at $y=0$ and at the center of the top rod. The averaged analytical field is also plotted.

Note that these equations are correct electrostatic models but a relativistic correction factor is necessary to include length contraction in z when simulating klystrons.

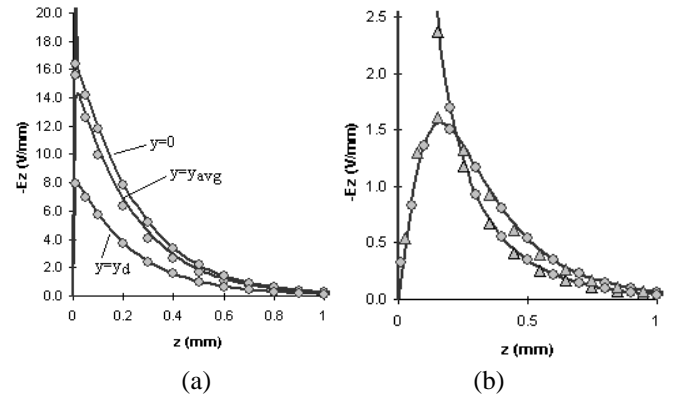


Fig. 6a. Comparison of equations (29) and (30) with simulated results (Solid Lines – Simulated Results, Filled Circles – Analytic Results).

Fig. 6b. Comparison of equations (31) and (32) with simulated results (Solid Lines – Simulated Results, Filled Circles – Equation (31), Filled Triangles – Equation (32)).

Testing the new space charge equations, Fig. 7 and Fig. 8 compare AJDISK with large signal simulation and small signal hand calculations [9] respectively. Excellent agreement is observed in both cases.

Fig. 7 compares the fundamental RF current calculated in AJDISK and MAGIC3D for the L-band sheet beam klystron [10]. MAGIC3D is a fully 3D PIC solver. A strong solenoid field was used in MAGIC3D to prevent transverse motion in the beam and provide a better comparison.

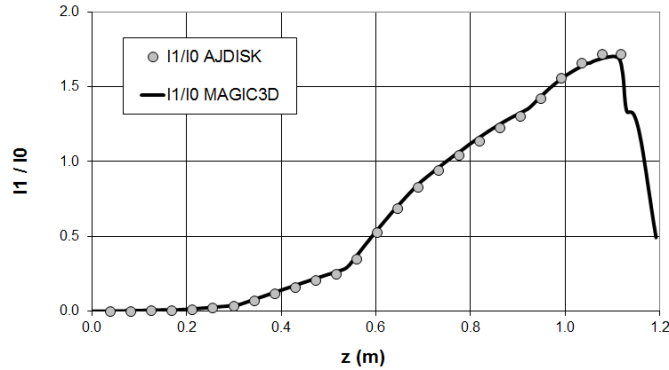


Fig. 7. I1/I0 comparison between MAGIC3D and AJDISK.

Fig. 8 compares AJDISK with small signal hand calculations for the ONR sheet beam klystron [11]. The slight error between results in Fig. 8 is primarily related to the difference in plasma reduction factor between the two calculations (the small signal analytic hand calculations assume an infinitely wide beam).

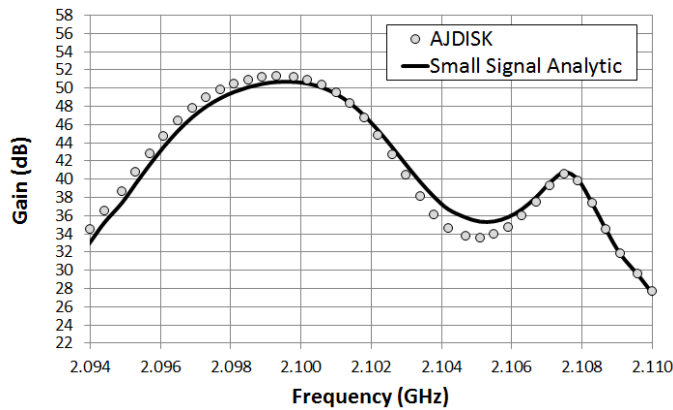


Fig. 8. Gain comparison between AJDISK and small signal analysis.

IX. AJDISK VS MEASUREMENT

Fig. 9 compares AJDISK with measured data of SLAC's W-band sheet beam klystron [2]. The results are in good agreement and it is believed that most of the error is due to the difficulty of maintaining tight mechanical tolerances at 95 GHz. A more thorough comparison of AJDISK with measurement will be conducted when the ONR sheet beam klystron is tested at SLAC.

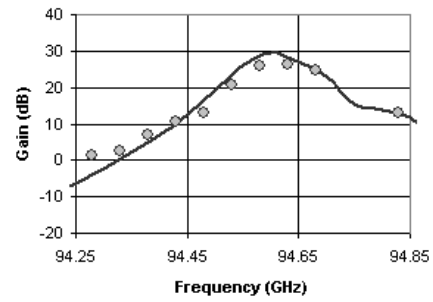


Fig. 9. Comparison of AJDISK with measurements from SLAC's W-band sheet beam klystron (Solid Line – AJDISK Simulation, Filled Circles - Measured Results)

X. CONCLUSION

The disk simulation algorithm provided in [3] and [4] was extended to sheet beam devices. It was shown that the algorithm could be extended to sheet beams by replacing the space charge equation for cylindrical beams with the space charge equation for rectangular beams. The sheet beam space charge equation was derived for simple plates and for rods (to allow velocity taper in the beam). The results were shown to be in good agreement with simulation.

The new space charge equations were implemented in SLAC's klystron simulator, AJDISK. AJDISK was used to simulate SLAC's W-band sheet beam klystron and good agreement was observed between the simulated results and measured results.

REFERENCES

- [1] A. J. Jensen, G. Caryotakis, G. Scheitrum, D. Sprehn, and B. Steele, "Sheet Beam Klystron Simulation Using AJDISK," *IEEE Vacuum Electronics*. April 25-27, 2006, pp. 489-490.
- [2] G. Scheitrum, G. Caryotakis, A. Burke, A. Jensen, E. Jongewaard, M. Neubauer, R. Phillips, D. Sprehn, and B. Steele, "W-band sheet beam klystron research at SLAC," *IEEE Vacuum Electronics*. April 25-27, 2006, pp. 481-482.
- [3] T. Kageyama, Y. Morizumi, and E. Watanabe, "A large-signal analysis of broad-band klystrons with design applications," *IEEE Trans. Electron Devices*, vol. ED-24, pp. 3-12, Jan. 1977.
- [4] P. J. Tallerico, "Design considerations for the high-power multicavity klystron," *IEEE Trans. Electron Devices*, vol. ED-18, pp. 374-382, June 1971.
- [5] T. Wessel-Berg, "Representation of gap fields by Gaussian functions," unpublished.
- [6] J. R. M. Vaughan, "The input gap voltage of a klystron," *IEEE Trans. Electron Devices*, vol. ED-32, pp. 2510-2511, Nov. 1985.
- [7] J. E. Rowe, *Nonlinear Electron-Wave Interaction Phenomena*. New York: Academic Press, 1965.
- [8] W. R. Smythe, *Static and Dynamic Electricity*. New York: McGraw-Hill, 1939.
- [9] K. H. Kreuchen, B. A. Auld, and N. E. Dixon, "A study of the broadband frequency response of the multicavity klystron amplifier," *Journ. Electronics*, pp. 529-567, May 1957.
- [10] D. Sprehn, E. Jongewaard, A. Haase, A. Jensen, and A. Burke "Development of a 10MW sheet beam klystron for the ILC," in Particle Accelerator Conf. (PAC), May 4-8, 2009.
- [11] A. Jensen, M. Fazio, A. Haase, E. Jongewaard, D. Martin, J. Neilson, D. Sprehn, A. Vlieks, "S-Band Sheet Beam Klystron Research and Development," in IEEE International Vacuum Electronics. May 21-23, 2013.